IMMERSED BOUNDARY METHOD FOR SIMULATIONS OF FLOWS AROUND CYLINDERS WITH FLUID AND STRUCTURE INTERACTION

Silva, A. R. calicers@hotmail.com
Lima, A. M. G. amglima@unifei.edu.br
Federal University of Itajubá
Campus José Rodrigues Seabra, Zip Code 37500-903 – Itajubá – MB Brazil

Silveira-Neto, A. aristeus@mecanica.ufu.br
Rade, D. A. domingos@ufu.br
Federal University of Uberlândia
Campus Santa Mônica, Zip Code 38400-902 – Uberlândia – MG Brazil

Francis, R. franciss@petrobras.com.br
Petrobras – Submarine Technology
Horácio de Macedo Av. 950, University City – Ilha do Fundão

Abstract. *Numerical analysis of incompressible flow over a stationary and an elastically mounted cylinder has been performed. The two-dimensional filtered Navier-Stokes equaltions with the Smagorinsky sub-grid scale model are solvee. The body in the flow was modeled by Immersed Boundary Methodology. In both case (stationary and mobile), the cylinders pair was disposed in different configurations. For the no stationary case, the displacement of the body was obtained by resolution of the harmonic model equation by the fourth order Runge-Kutta technique. The simulations were performed for Reynolds number equal to 72,000 for the stationary case and for three Reynolds numbers for the fluid-structure interaction case. The quantitative and qualitative results were analyzed and compared with literature'results. The results of the fluid-structure interaction is preliminary, being need new analyzes considering others parameters and less complexity. The methodology has showed promising in the simulation involving fluid structure interaction.*

Keywords*: Immersed Boundary Method, Fluid Structure Interaction, Circular Cylinder.*

1. INTRODUCTION

The flow over a pair of circular cylinders has been studied by many researchers and appears in a large number of engineering applications. Silva *et al.* (2003) have developed a study about flows over a configuration of several cylinders disposed in V arrangements, for low Reynolds number. The tandem and side-by-side arrangements are the most extensively studied in the literature (Lima e Silva *et al.*, 2007; Sumner *et al.*, 1999; Carmo and Meneghini, 2006; Meneghini *et al.*, 2001; Deng *et al.*, 2006). However, the most general form is the staggered arrangement (Sumner *et al.*, 2007; Sumner *et al.*, 2005).

The dynamic flow becomes more complex when the cylinders pair is allowed to move in the longitudinal and transversal directions to the flow. The fluid-structure interaction is a topic of great interest and has defined researches and guided projects through physical and numerical experiments and theoretical analyzes. In all of the cases, the aim is to better understanding, the prevention and prediction of the vortex induced vibration (VIV), in order to quantify the relation between the structure response and the parameters that it influence. This phenomenon occurs in many situations of engineering, such as bridges, transmission lines, surfaces of control of aircraft, maritime structures, drilling and production of oil, amongst other hydrodynamic and hidroacústica applications. A detailed review of the works which has been developed about fluid-structure interaction can be found in Silva (2008)

The main goal of the study is to have a better understanding of the flow around a bundle of risers, which are subjected to shear flow due to maritime currents. The flow around risers is very complex and changes in intensity and direction with the water depth. The interference of the flow around bluff bodies and the interference of a cylinder on the other are responsible for the changing in the characteristics of the fluid load acting over these immersed bodies. Furthermore, flow over circular cylinders is related to different fundamental fluid-dynamic phenomena, such as boundary-layer separation, shear-layer development and vortex dynamics (Akbari and Price, 2005).

The objective of the present paper is twofold: i) to apply the Immersed Boundary Methodology (MFI) to simulate the flow over stationary and mobile pair of cylinders; ii) to analyze the interference effect between each other on the drag coefficients and to characterize the mechanism of vortex shedding in various configurations. Regarding the simulation results, it is presented the vorticity contours and the comparative results of the drag coefficients for all analyzed Reynolds number. The outline of the paper is as follows: we first describe the mathematical model for incompressible flows together with the mathematical methodology in Section 2. In Section 3, we present the description of the problem and in the Section 4 we present the numerical results. Finally, in Section 5 the concluding remarks are presented.

NOMENCLATURE

C_d drag coefficient ($F_d/(0.5\rho U^2 d)$), dimensionless
C_l lift coefficient ($F_l/(0.5\rho U^2 d)$), dimensionless
d diameter of the cylinder, m
D distribution function, m^{-2}
f frequency of vortex shedding, s^{-1}
f_1, f_2 auxiliar functions to the distribution function, dimensionless
f_i *i-th* component of the Eulerian force, N/m^3
f Eulerian force vector, N/m^3
F Lagrangean force vector, N
F_a acceleration force vector, N
F_i inertial force vector, N
F_v viscous force vector, N
F_p pressure force vector, N
F_d drag force, N
F_l lift force, N
n superscript that indicates time
p pressure, N/m^2
r parameter of the distribution function, dimensionless
Re Reynolds number ($\rho U d/\mu$), dimensionless
S distance between the centers of the two cylinders, m
St Strouhal number (fd/U), dimensionless
t physical time, s
T dimensionless time (tU/d), dimensionless
u_i *i-th* component of the velocity, m/s
u_j *j-th* component of the velocity, m/s
U velocity of the free stream, m/s
$x = (x_i, y_j)$ Eulerian coordinate vector, m
$x = (x_k, y_k)$ Lagrangean coordinate vector, m

Greek Symbols

∇p pressure gradient, N/m^3
ΔS distance between two Lagrangean points, m
Δt time step, s
ϕ general variable of the Lagrangean polynomial function
ϕ incidence angle
ρ mass density, kg/m^3
μ dynamic viscosity, kg/(m.s)

Indexes

i, j indicate Eulerian mesh points
k indicate Lagrangean mesh points

2. MODELING METHODOLOGY

The methodology used in the present work is based on the Immersed Boundary Method (Peskin, 1977) associated with the Virtual Physical Model (Lima e Silva *et al*., 2007). This methodology is based on the Navier-Stokes equations with an added force source term. This force term acts so that the fluid perceives the existence of the immersed body, thus making the exchange of information between both domains. In this methodology a mixed Eulerian-Lagrangean formulation is used, where an Eulerian grid (fixed) describes the flow and a Lagrangean grid (which can be fixed or not) describes the immersed bodies. These meshes are geometrically independent, which allows the modeling of flows around complex, movable or deformable geometries without the need of any remeshing process. Both domains are physically coupled by a force field obtained at the Lagrangean points, which is then distributed over the Eulerian nodes in the body's neighborhood.

2.1. MATHEMATICAL FORMULATION FOR THE FLUID

The two-dimensional viscous, incompressible flows can be modeled by the filtered Navier-Stokes equations as follows:

$$\frac{\partial u_i}{\partial t}+\frac{\partial\left(u_i u_j\right)}{\partial x_j}=-\frac{1}{\rho}\frac{\partial p}{\partial x_i}+\frac{\partial}{\partial x_j}\left[\nu_{ef}\left(\frac{\partial u_i}{\partial x_j}+\frac{\partial u_j}{\partial x_i}\right)\right]+f_i, \tag{1}$$

$$\frac{\partial u_i}{\partial x_i}=0, \tag{2}$$

where ρ and ν_{ef} are the specific mass and the effective viscosity, respectively; u_i is the filtered velocity components, p is the filtered pressure and f_i is the component of the Eulerian vector force, which is calculated by the distribution of the components of the Lagrangean vector force as follows:

$$f_i\left(\vec{x}\right)=\sum_k D_{ij}\left(\vec{x}-\vec{x}_k\right)F_i\left(\vec{x}_k\right)\Delta S^2\left(\vec{x}_k\right), \tag{3}$$

In Eq. (3) $\vec{x}$ and $\vec{x}_k$ are the position vectors of the Eulerian and Lagrangean points, respectively, ΔS is the distance between two Lagrangean points, $F_i\left(\vec{x}_k\right)$ is the i-th component of the interfacial Lagrangean force and D_{ij} is the interpolation/distribution function, proposed by Peskin and McQueen (1994).

2.2. MATHEMATICAL FORMULATION FOR FLUID-SOLID INTERFACE

The Virtual Physical Model enables to calculate the Lagrangean force field based on the momentum balance over a fluid particle placed on the Lagrangean points. Applying Newton's second law to such a particle of fluid, the Lagrangean force is found to be given by:

$$\vec{F}\left(\vec{x}_k,t\right)=\underbrace{\rho\frac{\partial\vec{V}\left(\vec{x}_k,t\right)}{\partial t}}_{\vec{F}_a}+\underbrace{\rho\vec{\nabla}.\left(\vec{V}\left(\vec{x}_k,t\right)\vec{V}\left(\vec{x}_k,t\right)\right)}_{\vec{F}_i}\underbrace{-\vec{\nabla}.\left[\mu\left(\vec{\nabla}\vec{V}\left(\vec{x}_k,t\right)+\vec{\nabla}^T\vec{V}\left(\vec{x}_k,t\right)\right)\right]}_{\vec{F}_v}+\underbrace{\vec{\nabla}p\left(\vec{x}_k,t\right)}_{\vec{F}_p}, \tag{4}$$

where $\vec{F}_a$ is the force engendered by the particle acceleration, $\vec{F}_i$ is the inertial force, $\vec{F}_v$ is the viscous force and $\vec{F}_p$ is the pressure force. These terms are calculated using an approximation based on Lagrange polynomials. Details of the interpolation scheme for each component of the velocity and for pressure can be found in (Silva, 2008). Once obtained the force given by Eq. (4), it is distributed to Eulerian nodes according to Eq. (3), in order to obtain the Eulerian force field that accounts for the immersed bodies.

Turbulence model

The turbulence model used in the present paper is based on the filtering process, using the so-named box filter, as described by Silveira-Neto *et al*. (2002) and Silveira-Neto (2003). The turbulent viscosity is given as a function of the strain rate and the scale length as (Smagorinsky, 1963):

$$\nu_t = \left(C_S \ell\right)^2 \sqrt{2\overline{S_{ij}}\ \overline{S_{ij}}}, \tag{5}$$

$$\overline{S_{ij}} = \frac{1}{2}\left(\frac{\partial \overline{u_i}}{\partial x_j} + \frac{\partial \overline{u_j}}{\partial x_i}\right), \tag{6}$$

where $\ell = \sqrt{\Delta x \Delta y}$ is the characteristic sub-grid length, $\overline{S_{ij}}$ is the strain rate and C_S is the Smagorinsky constant. The analytical value for homogeneous and isotropic turbulence is $C_S = 0.18$ (Lilly, 1967). Here, the sub-grid turbulent viscosity plays the role of stabilizing the numerical instabilities. In the present work, these instabilities are characteristics of the central difference scheme, which is used for both advective and diffusive terms.

In all simulations a damping function was used in the outlet of the domain. This function absorbs the vortex in the outlet, avoiding reflections that could propagate from the outlet towards the inlet of the domain. This function is given by (Meitz and Fazel, 2000):

$$g(\varepsilon) = 1 - 6\varepsilon^5 + 15\varepsilon^4 - 10\varepsilon^3, \tag{7}$$

$$\varepsilon = \frac{\mathrm{i} - \mathrm{i}_1}{\mathrm{i}_2 - \mathrm{i}_1}, \tag{8}$$

where *i* is the grid number. The points i_1 and i_2 ($i_1 \le i \le i_2$) indicate the initial and final grid points of the damped zone.

3. NUMERICAL METHOD

The momentum and continuity equations are numerically solved by using the finite difference method through the fractional step method based on the pressure correction concept (Chorin, 1968). Given the initial velocity, the pressure and the force fields, an estimated velocity field is obtained. These velocity field is used to calculate the pressure correction, solving a system of linear algebraic equations, for which the *MSI* (Modified Strongly Implicit Procedure), developed by Scheneider and Zedan (1981), is used. The Poisson equation gives the coupling between Eqs. (1) and (2). Also, it provides values of pressure that allow that the velocities components, obtained using the Navier-Stokes equations, satisfy the mass conservation condition. The time discretization is done by the second order Runge-Kutta method. The estimation of the velocity is explicitly calculated as follows:

$$\frac{\tilde{u}_i^{\,n+1} - u_i^n}{\Delta t} = -\frac{1}{\rho}\frac{\partial p^n}{\partial x_i} - \left[\frac{\partial\left(u_i u_j\right)}{\partial x_j}\right]^n + \frac{\partial}{\partial x_j}\left[\nu_{ef}\left(\frac{\partial u_i}{\partial x_j} + \frac{\partial u_j}{\partial x_i}\right)\right]^n + f_i^{\,n}, \tag{9}$$

where $\tilde{u}_i$ is the estimated velocity component, Δt is the computational time step and n is the substep index.

The Poisson equation for pressure correction, p'^{n+1}, with the source term given by the divergent of the estimated velocity, is given by:

$$\nabla^2 p'^{n+1} = \frac{\rho}{\Delta t}\vec{\nabla}.\vec{\tilde{u}}^{\,n+1}. \tag{10}$$

The velocity field is updated by solving the following equation:

$$u_i^{n+1} = \tilde{u}_i^{n+1} - \frac{\Delta t}{\rho}\frac{\partial p'^{\,n+1}}{\partial x_i}. \tag{11}$$

The previous pressure field p^n and the correction pressure p'^{n+1} are used to calculate the updated values of the pressure field, according to:

$$p^{n+1} = p^n + p'^{n+1}. \tag{12}$$

4. PROBLEM DESCRIPTION AND NUMERICAL RESULTS

In the present study, the cylinders are assumed to have equal diameters d and the distance between their centers is designated by L for all arrangements. The angle between the flow direction and the line connecting the centers of the cylinders is varied. In all the simulated cases, the pair of cylinders is symmetrically placed in a uniform grid.

For the stationary case, the simulations were performed at Reynolds numbers Re=72,000. The dimensionless time was defined as $T = tU/d$, where t is the physical time, given in seconds. The time step was set as $\Delta t = 1.10^{-5} s$ at the first iteration and was increased gradually up to $\Delta t = 1.10^{-3} s$ during the first 100 iterations. After that, the time step was calculated so that the stability criterion is attained. The grid used was composed by 600x300 points in *x* and *y* directions, respectively.

For the fluid-structure interaction case, one considers the two-dimensional circular cylinders with mass m per unit lenght which is tethered by a linear spring of stiffness k and a linear viscous damper of coefficient *c* to the fixed space. In the case characterized herein as having only two degree-of-freedom (2 dof), the cylinder displacement is assumed to be restrained in such a way that the motion in the longitudinal and transversal directions to the flow is allowed. Thus, from the dynamics standpoint, the cylinder movement can be modeled considering a traditional linear mass-spring-damper system (Meirovitch, 1989; Thomson and Dahlen, 1998) subjected to the forces exerted by the fluid.

The movement equations of the cylinder for two degree of freedoms, are expressed by:

$$m\ddot{y} + c\dot{y} + ky = F_l(t) \tag{13}$$

$$m\ddot{x} + c\dot{x} + kx = F_d(t) \tag{14}$$

where x and y are the longitudinal and transversal displacement and $F_d(t)$ e $F_l(t)$ are the longitudinal and transversal excitation forces, respectively. These equations were solved using a fourth order Runge-Kutta integration scheme.

4.1. ALGORITHM FOR NUMERICAL RESOLUTION

The iterative algorithm used for performing the computations can be summarized according to the following steps:

1. The mathematical model for the fluid (Eqs. 1 and 2) is solved using the Finite Differences Method;
2. The Cartesian components of the Lagrangean forces that acts over the cylinder, $\vec{F}_x$ and $\vec{F}_y$ are obtained using Eq. (4);
3. The components of forces in directions longitudinal and transversal to the flow are obtained using expressions $F_l = \sum \vec{F}_y(\vec{y}_k, t)\Delta S^2$ and $F_d = \sum \vec{F}_x(\vec{x}_k, t)\Delta S^2$, respectively;
4. The equations of motion (13 and 14) are solved by using a fourth order Runge-Kutta method, providing the velocity and the position of the center of mass of the cylinder.
5. The position of the cylinders inside the fluid domain is updated;
6. Time is advanced by one step.

4.2. RESULTS FOR THE STATIONARY CYLINDER CASE

Characteristics of vortex shedding

In order to investigate the effect of the cylinders proximity on vortex shedding, simulations were performed for cylinders in tandem, staggered and side-by-side arrangements. For all cases, the pitch ratio was assumed to be *L/D*=2. The vorticity contours shown in Fig. 1 put in evidence very interesting characteristics of the flow as the angle between the cylinders changes. In Fig. 1(a), it can be observed that for the tandem arrangement, the shear layers of cylinder A involves cylinder B with only one vortex wake formed behind the downstream cylinder. The interaction between the two shear layers occurs only behind cylinder B, which is inside the wake of cylinder A. There is a '2S' mode of vortex

shedding, composing the classical Von Kármán Street. According to Naudascher and Rockwell (1994), vortex shedding behind the upstream cylinder (in the present case cylinder A) is not perceived for pitch ratios smaller than 3.8. In their study at low Reynolds number (Re = 220), Deng et al. (2006), concluded that for two-dimensional simulations, each cylinder yielded a vortex wake only for $L/D \geq 4.0$. They also affirmed that, even in three-dimensional flows for this configuration and $L/D \leq 3.5$, the flow is quasi two-dimensional.

For the tandem arrangement and ϕ=7°, the downstream cylinder is inside the wake of the upstream cylinder. For $7° < \phi \leq 15°$, the internal shear layer from the upstream cylinder collides with the frontal part of the downstream cylinder. As the incidence angle increases, the vortex wake becomes irregular behind the cylinder B. For ϕ=7°, the '2S' mode of vortex shedding is observed. Increasing the angle ϕ, vortices pairs as well as single vortices are observed, composing the wake, as shown in Fig. 1(d). Figures from 1(e) to 1(g) show a different behavior of the flow. In the region near the cylinders, two wakes are formed: the wake from cylinder A is narrow, while the wake from the cylinder B is wide. However, it is not possible to classify the vortex shedding mode. The wake becomes complex and very disorganized. It should be noted that these vorticity fields are qualitatively similar to the standard behavior show in Sumner et al. (2005).

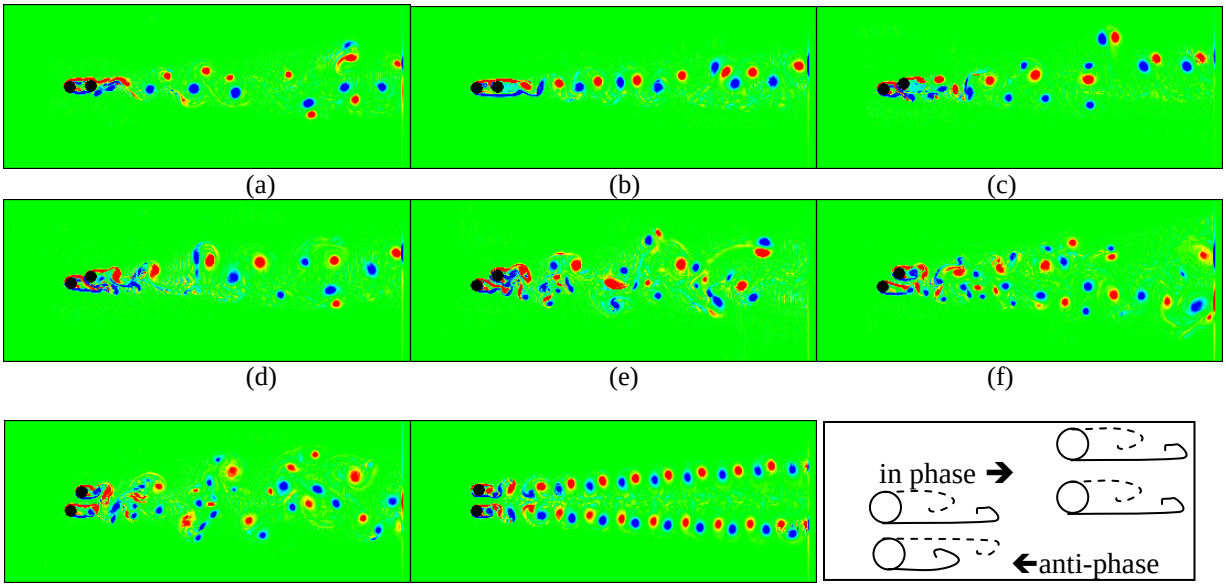

Figure 1. Vorticity contours for Re = 72,000: a) $\phi = 0°$; b) $\phi = 7°$; c) $\phi = 11°$; d) $\phi = 15°$; e) $\phi = 30°$; f) $\phi = 45°$; g) 60°; h) $\phi = 90°$; i) illustrative scheme of vortex shedding in phase and anti-phase.

Simulations have also been performed with two circular cylinders in a side-by-side arrangement for the same pitch ratio and the same Reynolds number. In this configuration, the line defined by the centers of the two cylinders is oriented perpendicularly to the oncoming flow. For this case, the classification of vortex shedding in phase or anti phase, adopted in the present work, is the same used by Wang and Zhou (2005). This classification is illustrated in Fig. 1(i). An anti-phase wake, with symmetric vortex shedding around the central line of the flow, can be observed in Fig. 1(h). As time passes, it is observed a gap between the two wakes at approximately 10*D* downstream of the cylinders. Anti-phase wake was also observed by other authors at other Reynolds number and pitch ratio. Wang and Zhou (2005) verified this behavior for pitch ratio equal to 3 and Re = 5,900. According to those authors, the anti-phase vortex shedding is relatively stable, while the in-phase vortex shedding mode is unstable. Meneghini *et al.* (2001) also observed this behavior for pitch ratio equal to 3 at low Reynolds number.

In the following, the mean values of the dynamic coefficients, for the upstream and downstream cylinders, are compared with the experimental results provided by Sumner *et al.* (2005) for pitch ratio equal to 2 and Reynolds number equal to 72,000 for different incidence angles. Figure 2(a) shows the mean values of the drag coefficient for cylinder A. For $\phi < 15°$, the C_d decreases slightly and then increases gradually with the increase of ϕ. For $\phi \leq 65°$, the mean values of the drag coefficient are smaller than for single cylinder ($C_d = 1.17$) with differences up to 27%. For $\phi > 65°$ the mean values of C_d are larger than for a single cylinder, with a maximum difference of 11%. For $\phi = 90°$, the maximum value of the drag coefficient (20% greater than to for a single cylinder) was obtained.

For the downstream cylinder (cylinder B), considered in Fig. 2(b), the mean values obtained for the drag coefficient are positive in the entire range of incidence angle and it increase gradually, as this angle increases. In the research work

reported herein, negative values of the drag coefficient were not obtained, as opposed to what can be observed in the experimental results reported by Sumner *et al*., (2005). On the other hand, for high values of ϕ, the present results show quite good agreement with the experimental results. It is believed that the differences between results obtained in the two works can be reduced by the use of more accurate turbulence models, as well as by performing full three-dimensional simulations.

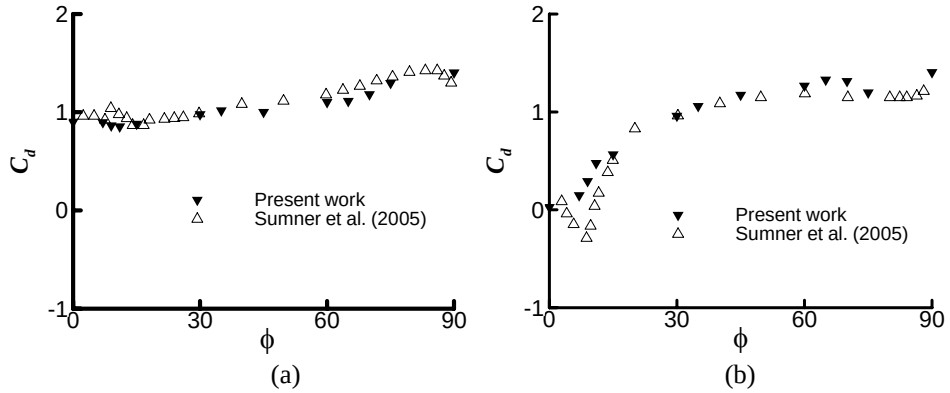

Figure 2. Mean drag coefficients versus ϕ for Re = 72,000: (a) cylinder A; (b) cylinder B.

Figure 3 shows the mean values of the lift coefficient C_l. Figure 3(a) shows the variations of the mean values of this coefficient for the upstream cylinder, which take values close to zero, for mount angles $\phi < 75°$, and values different from zero in the range $75° \le \phi \le 90°$. On the other hand, for the downstream cylinder considered in Fig. 3(b), the mean values of the lift coefficient increase up to $\phi = 15°$. After that, the values of the mean lift coefficient decrease for mount angles up to $\phi = 45°$. For $\phi > 45°$, the mean values of C_l are positive. The present results, for upstream cylinder, showed good agreement with the experimental results for the entire range of ϕ. On the other hand, for the downstream cylinder, the agreement of the results obtained for $\phi < 15°$ with those presented by Sumner *et al*. (2005) is not satisfactory. Further developments are needed to confirm this point.

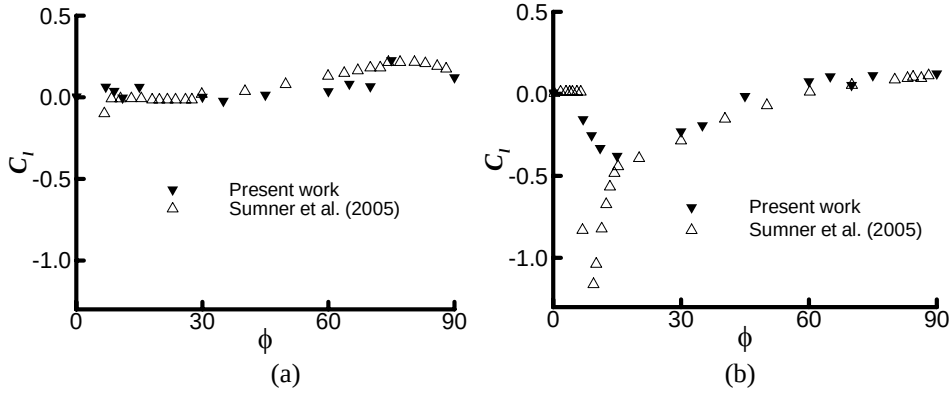

Figure 3. Mean lift coefficients versus ϕ for Re = 72,000: (a) cylinder A; (b) cylinder B.

4.3. RESULTS FOR THE MOVING CYLINDERS CASE

In order to investigate the effect of the cylinders proximity on hydrodynamic forces for moving circular cylinders case, simulations were performed for cylinders in tandem, staggered and side-by-side arrangements for three values of Reynolds number. In order to compare the drag forces with the experimental results provided by PETROBRAS, the structural parameters and pitch ratio in the present study were the same used in experiments. For all cases, the pitch ratio was assumed to be *L/D*=3, the damping ratio was equal to 0.01 and the stiffness of spring equal to 390N/m. Due to large quantity of date, will be presented only the vorticity contours for Reynolds number 41,900.

Characteristics of vortex shedding

Figure 4 shows the flow visualization by the vorticity contours. For the tandem arrangement, Fig. 4(a), it can be verified the shedding vortex process behind both cylinders, resulting in a single wake downstream of the cylinder B.

This behavior was not noted for the stationary cylinder case, Fig. 1(a), for pitch ratio equal to 2. The '2S' mode of vortex shedding is herein. Increasing the angle between the cylinders for $\phi = 15°$, Fig. 4(b), it can be observed vortices pair composed by the positive vortice from the upstream cylinder and the negative vortice from the downstream cylinder. It can also be noted single vortices composing the wake. For $\phi = 30º$, Fig. 4(c), the vortices wake are not well defined. These wakes are more complex and disorganized than the previous. Increasing the angle to $\phi = 60º$, Fig. 4(d), it can be noted two independent wakes in relation to the central axis of the flow. This behavior is more pronounced for $\phi = 90º$, where may be observed the anti-phase vortex shedding process with symmetrical wakes in relation to the central axis of the flow. The vortex shedding process influences the forces acting over the cylinders, as well in the response of them. .

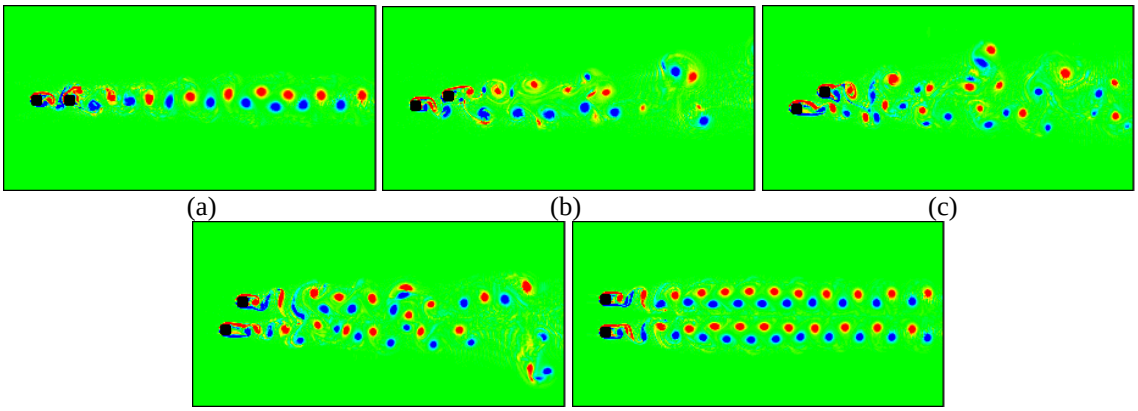

Figure 4. Vorticity contours for Re = 41,900: a) $\phi = 0°$; b) $\phi = 15°$; c) $\phi = 30°$; d) $\phi = 60°$; and) $\phi = 90°$.

Figure 5 shows the mean values of the drag coefficient for the cylinder A, for three values of Reynolds number comparing with the experimental results provided by CENPES. It can be noted in Fig. 5(a), that the mean values are lower than the experimental results for all interval of angle. The mean drag reduce with increase in the angle from $\phi = 0º$ to $\phi = 30º$, and after increase. The behavior presented by both results is the same.

Increasing the Reynolds number to 83,700, Fig. 5(b) the mean value of the drag coefficient for the tandem arrangement had reduced comparing the previous Reynolds number, while, for the other angles, the both results had presented good agreement. In order to verify the influence of Reynolds number in the drag mean values, simulations at Reynolds equal to 105,000 were carried out. It is noted in Fig. 5(d), that although the results have distanced themselves from a little, it can be considered reasonable, comparing the results of Fig. 5(a).

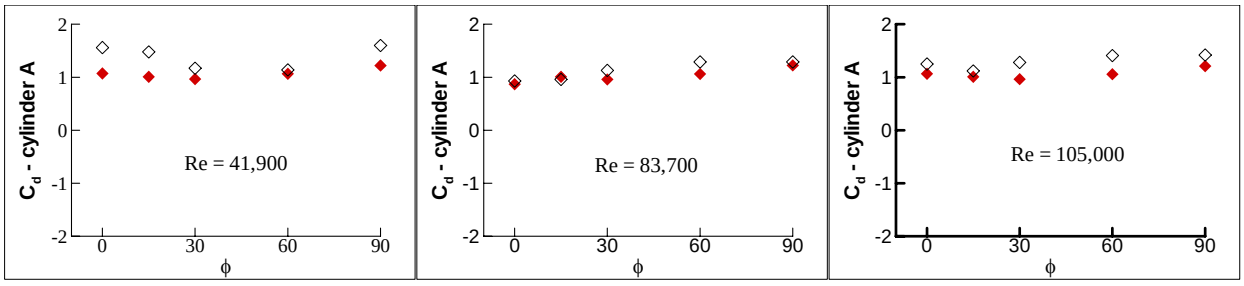

Figure 5. Mean drag coefficients for the cylinder A in function of ϕ: full symbols – present work and empty symbols – CENPES'results.

For the downstream cylinder, Fig. 6, it is observed in the both results, that the drag mean values increase as the angle increase up to ϕ=60º and reduce for ϕ=90º. For the tandem arrangement, the mean value has presented a considerable reduction with the increase in the Reynolds number, Fig. 6(b), while, keep practically unchanged for ϕ>0º. For this Reynolds number the results has presented better concordance. In Fig. 6(c), the results presented similar behavior for $\phi \leq 60º$.

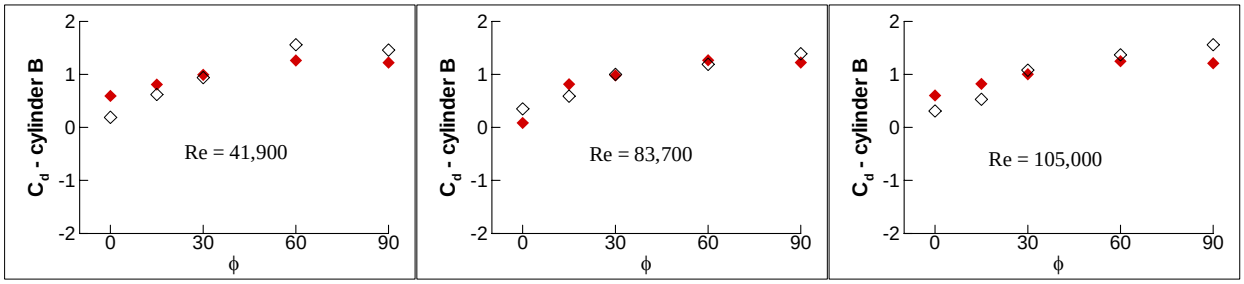

(a) (b) (c)

Figure 6. Mean drag coefficients for the cylinder B in function of ϕ : full symbols – present work and empty symbols – CENPES'results.

It is interesting to note in Fig. 6, that for tandem arrangement, the drag mean value has presented a considerable reduction with increase in the Reynolds number from 41,900 to 83,700 and an increase with further increase in Reynolds number to 105,000. This behavior probably is due to the dynamic of the flow for this configuration, as shown in Fig. 7. For Re=41,900, Fig. 7(a), it can be noted the vortex shedding process downstream of cylinder A, as already commented. This behavior is not observed for Re=83,700 in Fig. 7(b), comparing the same dimensionless time ($T=tU/D$). The both cylinders have presented as a single bluff body and the vortices wake oscillates. For Re=105,000, the dynamic flow is similar that observed for Re=41,900.

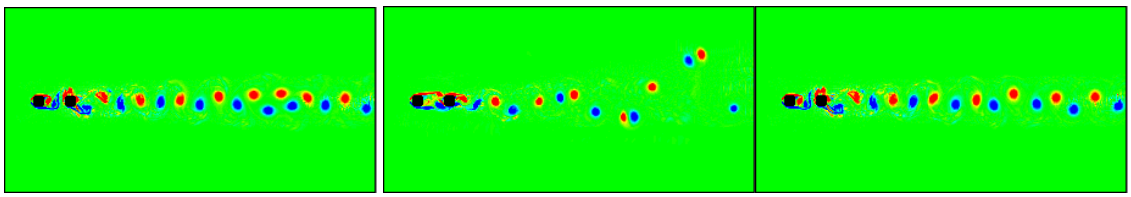

(a) (b) (c)

Figure 7. Vorticity contours for $\phi = 0°$: a) Re=41,900; b) Re=83,700 and c) Re=105,000.

5. CONCLUDING REMARKS

In the present work, an extensive numerical investigation about interference effects between two circular cylinders in the subcritical Reynolds number regime, Re = 72,000 was undertaken. The investigation has been extended to simulations with cylinders pair supported elastically for three Reynolds number. In both case the pair of circular cylinders has equal diameters and was arranged in different configurations. The vorticity contours, for pitch ratio equal 2 and the incidence angle ϕ varying from 0° to 90° were presented. The variations of the dynamic coefficients were related to the changes in the flow patterns as change the cylinder configurations. It was verified that these behaviors are more significant on the dynamic coefficients of the downstream cylinder as compared with the upstream cylinder. The results for the upstream cylinder presented good agreement with the experimental results obtained by Sumner *et al.* (2005) for all incidence angles considered. Nonetheless, for the downstream cylinder the results must be improved, although they presented good agreement with experimental counterparts for $\phi > 15°$. The difference between the numerical and experimental results can be attributed mainly to the two-dimensionality of the simulations.

The presented results involving flow induced vibration are preliminary. In general, the results of this work is promising, giving to different assumptions adopted, the methodology, the turbulence model and two-dimensionality. New simulations will be need, including involving less complexity, for example, a cylinder with just two degrees of freedom, a cylinder fix and mobile, as well as two mobile cylinders with one degree of freedom. Therefore, the primary goal is the quest for a better understanding of the flow dynamics for problems involving fluid-structure interaction and understanding the influence of the cylinders movement in the fluid and bodies response.

6. ACKNOWLEDGEMENTS

The authors acknowledge CNPq (National Council for Scientific and Technological Development -Brazilian Ministry of Technology), PETROBRAS and School of Mechanical Engineering of Federal University of Uberlândia – MG.

7. REFERENCES

Akbari, M. H.; Price, S. J., 2005, "Numerical investigation of flow patterns for staggered cylinder pairs in cross-flow", *Journal of Fluids and Structures*, 20, pp. 533-554.

Carmo, B. S.; Meneghini, J. R., 2006, "Numerical investigation of the flow around two circular cylinders in tandem", *Journal of Fluids and Structures***.** 22, pp 979-988.

Chorin, A., 1968, "Numerical solution of the Navier-Stokes equations", *Math. Comp*. 22, pp 745–762.

Deng, J.; Ren, A-L.; Zou, J-F.; Shao, X-M., 2006, "Three-dimensional flow around two circular cylinders in tandem arrangement". *Fluid Dynamics Research.* 38, pp 386-404.

Lilly, D.K., 1967, "The representation of small-scale Turbulence in Numerical Experiments", *Proc. IBM Sci, Comp. Symp. Environ. Sci, IBM Data Process. Did., White Plains. NY*, pp 195-210.

Lima e Silva, A. L. F.; Silveira-Neto, A.and Damasceno, J. J. R.., 2003, "Numerical Simulation of Two Dimensional Flows over a Circular Cylinder using the Immersed Boundary Method". *Journal of Computational Physics.* 189, pp 351-370.

Lima e Silva, A. L. F.; Silva, A. R.; Silveira-Neto, A. Numerical Simulation of Two-Dimensional Complex Flows around Bluff Bodies using the Immersed Boundary Method. **J. of the Braz. Soc. Of Mech. Sci. & Eng.** 4, pp 378-386, 2007.

Meirovitch, L. **Dynamics and Control of Structures**. John Wiley & Sons, 1989. 425p.

Meitz, H.L. and Fasel, H.F., 2000, "A compact-different scheme for the Navier-Stokes equations in vorticity-velocity formulation", *Journal of Computational Physics*, 157, pp 371-403.

Mengehini, J. R.; Saltara, F.; Siqueira, C. L. R.; Ferrari JR, J. A., 2001, "Numerical simulation of flow interference between two circular cylinders in tandem and syde-by-syde arrangements", *Journal of Fluids and Structures***.** 15, pp 327-350.

Naudascher, E.; Rockwell, D., 1994, *Flow-Induced Vibrations: An Engineering Guide*. Dover Publications, Inc. Mineola, New York, 414p.

Peskin, C.S., 1977, "Numerical Analysis of Blood Flow in the Heart", *Journal of Computational Physics***.** 25, pp 220-252.

Peskin, C. S.; McQueen, D. M., 1994, "A General Method for the Computer Simulation of Biological Systems Interacting with Fluids". SEB Symphosium on Biological Fluid Dynamics, Leeds, England, July 5-8.

Schneider, G. E.; Zedan, M. A., 1981, "Modified Strongly Implicit Procedure for the Numerical Solution of Field Problems". *Numerical Heat Transfer*, 4, 1.

Silva, A.R., Lima e Silva, A.L.F. and Silveira-Neto, A.,2003, "Modelagem Matemática e simulação Numérica de escoamentos sobre bancos de cilindros imersos dispostos em diferentes ângulos", *VI Congresso Íbero-Americano de Engenharia Mecânica*, Coimbra-Portugal.

Silva, A. R., 2008, "**Modelagem Matemática de Interação Fluido-Estrutura Utilizando o Método da Fronteira Imersa**" Tese de Doutorado. Universidade Federal de Uberlândia, Uberlândia.

Silveira-Neto, A., Mansur, S.S., and Silvestrini, J.H., 2002, "Equações da Turbulência: Média versus filtragem", III Escola da Turbulência.

Silveira-Neto, A., 2003, personal notes, "Apostila do curso de Turbulência".

Smagorinsky, J., 1963, "General Circulation Experiments with Primitive Equations", *Mon. Weather Rev*, v. 91, pp 99-164.

Sumner, D.; Richards, M. D.; Akosile, O.O, 2007, "Strouhal number data for two staggered circular cylinders". *J. Wind Eng. Ind. Aerodyn*., doi:10.1016/j.jweia.2007.06.013.

Sumner, D.; Rechards, M. D.; Akosile, O.O., 2005, "Two staggered circular cylinders of equal diameter in cross-flow", *Journal of Fluids and Structures***.** 20, pp 255-276.

Sumner, D.; Price, S. J.; Païdoussis, M.P., 1999, "Tandem cylinders in impulsively started flow", *Journal of Fluids and Structures***.** 13, pp 955-965.

Thomson, W. T.; Dahleh, M. D. **Theory of vibration with applications**. Prentice Hall, New Jersey, 1998. 524p.

Wang, Z. J.; Zhou, Y., 2005, "Vortex interactions in a two side-by-side near-wake", *International Journal of Heat and Fluid Flow*, 26, pp 362-377.